

การปลูกและวัดลักษณะสมบัติของควอนตัมดอตชนิดอินเดียมอาร์เซไนด์ที่มีการจัดเรียงตนเองบนแผ่นฐานเสมือน  
ซึ่งมีผิวหน้าชนิด cross-hatch



นางสาวโซ โซ เท็ด

วิทยานิพนธ์นี้เป็นส่วนหนึ่งของการศึกษาตามหลักสูตรปริญญาวิทยาศาสตรดุษฎีบัณฑิต  
สาขาวิชาวิศวกรรมไฟฟ้า ภาควิชาวิศวกรรมไฟฟ้า  
คณะวิศวกรรมศาสตร์ จุฬาลงกรณ์มหาวิทยาลัย  
ปีการศึกษา 2549  
ลิขสิทธิ์ของจุฬาลงกรณ์มหาวิทยาลัย

GROWTH AND CHARACTERISATION OF ORDERED INDIUM ARSENIDE QUANTUM DOTS ON  
CROSS-HATCH VIRTUAL SUBSTRATE

Miss. Cho Cho Thet

A Dissertation Submitted in Partial Fulfillment of the Requirements  
for the Degree of Doctor of Philosophy Program in Electrical Engineering

Department of Electrical Engineering

Faculty of Engineering

Chulalongkorn University

Academic Year 2006

Copyright of Chulalongkorn University

**491885**

Thesis Title GROWTH AND CHARACTERISATION OF ORDERED INDIUM  
ARSENIDE QUANTUM DOTS ON CROSS-HATCH VIRTUAL  
SUBSTRATE

By Miss. Cho Cho Thet

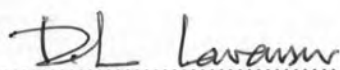
Department Electrical Engineering

Thesis Advisor Associate Professor Songphol Kanjanachuchai, Ph.D.

Thesis Co-advisor Professor Shunri Oda, D.Eng.

---

Accepted by the Faculty of Engineering, Chulalongkorn University in Partial  
Fulfillment of the Requirements for the Doctoral Degree



.....Dean of the Faculty of Engineering

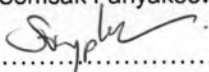
(Professor Direk Lavansiri, Ph.D.)

THESIS COMMITTEE



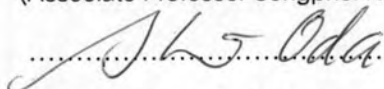
..... Chairman

(Professor Somsak Panyakeow, D. Eng.)



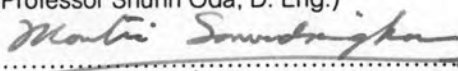
..... Thesis Advisor

(Associate Professor Songphol Kanjanachuchai, Ph.D.)



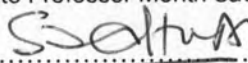
..... Thesis Co-advisor

(Professor Shunri Oda, D. Eng.)



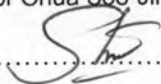
..... Member

(Associate Professor Montri Sawadsaringkarn, D.Ing.)



..... Member

(Professor Chua Soo-Jin, Ph.D.)



..... Member

(Sakuntam Sanorpim, Ph.D.)

ไซ ไซ เท็ต : การปลูกและวัดลักษณะสมบัติของควอนตัมดอตชนิดอินเดียมอาร์เซไนต์ที่มีการจัดเรียงตนเองบนแผ่นฐานเสมือนซึ่งมีผิวหน้าชนิด cross-hatch. (GROWTH AND CHARACTERISATION OF ORDERED INDIUM ARSENIDE QUANTUM DOTS ON CROSS-HATCH VIRTUAL SUBSTRATE) อ. ที่ปรึกษา : รศ.ดร. ทรงพล กาญจนชูชัย, อ. ที่ปรึกษาร่วม Dr. Shunri Oda, 115 หน้า

วิทยานิพนธ์ฉบับนี้ นำเสนอผลการปลูกโครงสร้างควอนตัมดอตบนรูปแบบตาราง (cross-hatch) ผิวหน้าแผ่นฐานเสมือน (virtual substrate, VS) ซึ่งเกิดจากการปลูก  $\text{In}_x\text{Ga}_{1-x}\text{As}$  บน  $\text{GaAs}$  (001) ด้วยเครื่องปลูกผลึกแบบลำโมเลกุล (molecular beam epitaxy, MBE) โดยได้ทำการพัฒนาแบบจำลองที่สามารถอธิบายถึงการเกิดการจัดเรียงควอนตัมดอต นอกจากนี้ยังใช้กล้องจุลทรรศน์แรงอะตอม (Atomic force microscopy, AFM) ในการศึกษาผิวหน้าของแผ่นฐานเสมือน และใช้กล้องจุลทรรศน์อิเล็กตรอนแบบส่งผ่าน (transmission electron microscopy, TEM) ในการวิเคราะห์หาต้นกำเนิดการเรียงตัวของควอนตัมดอต

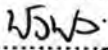
โครงสร้างตารางเกิดจากสารประกอบ  $\text{In}_{0.15}\text{Ga}_{0.85}\text{As}$  หนา 50 นาโนเมตรที่ถูกปลูกบนแผ่นฐาน  $\text{GaAs}$  หน้าตัด 001 ซึ่งมีความบกพร่องอันเนื่องมาจากค่าความต่างของค่าคงตัวผลึกซึ่งสามารถยืนยันได้ด้วย TEM การเปล่งฟูเรียมและการกวาดเส้นที่แสดงให้เห็นถึงผิวหน้ารูปแบบตารางมีการแสดงผลอย่างไม่เป็นคาบด้วยค่าความต่างเฉลี่ยของระยะทางในแนวข้างของทิศทาง [110] และ [1-10]

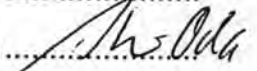
ปริมาณความเครียดและอัตราส่วนอินเดียมของแผ่นฐานเสมือน ที่สามารถตรวจสอบได้ด้วยเครื่องฉายรังสีเอ็กซ์ความละเอียดสูง (high resolution x-ray diffraction, HRXRD) พบว่าระดับการคลายความเครียดของ  $\text{InGaAs}$  ขึ้นอยู่กับความหนาและอัตราส่วนอินเดียม ดังนั้นควอนตัมดอตที่ปลูกบนชั้น  $\text{InGaAs}$  ที่แตกต่างกันทำให้เกิดการจัดเรียงตัวของควอนตัมดอตที่แตกต่างกันด้วย โดยจะได้ควอนตัมดอตเรียงแถวเมื่อความหนาของ  $\text{In}_{0.15}\text{Ga}_{0.85}\text{As}$  เท่ากับ 50 นาโนเมตร และจะได้กลุ่มของควอนตัมดอตโมเลกุลเมื่อความหนาดังกล่าวเปลี่ยนไปเป็น 100-150 นาโนเมตร โดยที่ผลการวัดคุณสมบัติทางแสงด้วยระบบโฟโตลูมิเนสเซนส์สอดคล้องกับผลจาก HRXRD

นอกจากนี้ยังได้ศึกษาผลกระทบของระยะเวลาหน่วงของการปลูก (Growth Interruption, GI) หลังจากควอนตัมดอตก่อตัวขึ้น เพื่อปรับปรุงขนาดของดอตให้สม่ำเสมอ จากการทดลองพบว่าเวลาหน่วง 30 วินาที เป็นเวลาที่เหมาะสมที่สุดสำหรับโครงสร้าง  $\text{InAs}$  ควอนตัมดอตบนแผ่นฐานเสมือนซึ่งมีผิวหน้าเป็น  $\text{In}_{0.15}\text{Ga}_{0.85}\text{As}$  นอกจากนี้ยังได้ทำการปลูกกลบควอนตัมดอตด้วยชั้น  $\text{GaAs}$  บางๆ เพื่อศึกษาลักษณะผิวหน้าซึ่งอาจถูกใช้เป็นแม่แบบสำหรับการปลูกในชั้นถัดไป จากการทดลองกลบชั้นบางพบว่า จะเกิดนาโนไฮลขึ้นบนควอนตัมดอตที่ก่อตัวบน  $\text{GaAs}$  แต่จะไม่เกิดขึ้นในกรณีที่เป็นการกลบควอนตัมดอตที่ก่อตัวบนรูปแบบตาราง โดยกลับพบควอนตัมดอตที่จัดเรียงตัวเองในทิศทาง [1-10] มากกว่าในทิศทาง [110] ซึ่งเป็นผลมาจากความไม่เที่ยงพอและความไม่สมมาตรของพลังงานความเครียดในระนาบที่ทำการปลูกควอนตัมดอต

ภาควิชา.....วิศวกรรมไฟฟ้า.....  
สาขาวิชา.....วิศวกรรมไฟฟ้า.....  
ปีการศึกษา .....2549.....

ลายมือชื่อนิสิต .....  .....

ลายมือชื่ออาจารย์ที่ปรึกษา .....  .....

ลายมือชื่ออาจารย์ที่ปรึกษาร่วม .....  .....

##4671853321 : MAJOR ELECTRICAL ENGINEERING

KEY WORD: ORDERED InAs QUANTUM DOTS / InGaAs / GaAs CROSS-HATCH / VIRTUAL SUBSTRATE / MOLECULAR BEAM EPITAXY

CHO CHO THET:GROWTH AND CHARACTERISATION OF ORDERED INDIUM ARSENIDE QUANTUM DOTS ON CROSS-HATCH VIRTUAL SUBSTRATE. THESIS ADVISOR: ASSOC. PROF. DR. SONGPOL KANJANACHUCHAI.THESIS CO-ADVISOR: PROF. DR. SHUNRI ODA, pp 115.

Growth of InAs quantum dots (QDs) on  $\text{In}_x\text{Ga}_{1-x}\text{As}/\text{GaAs}$  (001) cross-hatch virtual substrates (VS) has been carried out by molecular beam epitaxy (MBE). A model explaining the origin of QD alignment on the VS is developed. Cross-hatch surface morphology of the VS is studied by atomic force microscopy (AFM), and its origin by cross-sectional transmission electron microscopy (TEM).

The cross-hatch VS consists of 50-nm thick  $\text{In}_{0.15}\text{Ga}_{0.85}\text{As}$  on GaAs (001). Cross-hatch morphology on the surface of the VS is revealed by AFM and its origin from the networks of misfit dislocations (MDs) is confirmed by TEM. Fast Fourier transform (FFT) and line scan analyses indicate that the cross-hatch is aperiodic with different average lateral spacings in the two orthogonal ([1-10] and [110]) directions.

The strain and In composition of the VS are examined by high resolution X-ray diffraction (HRXRD). It is found that the degree of strain relaxation of the InGaAs layer increases with increasing thickness and In composition. Consequently, QDs grown on the different InGaAs layers result in different arrangements of QDs on the cross-hatch surfaces: ordered QDs are obtained when they are grown on partially-relaxed  $\text{In}_{0.15}\text{Ga}_{0.85}\text{As}$  (50 nm) layer; and groups of QDs are obtained when they are grown on more relaxed  $\text{In}_{0.15}\text{Ga}_{0.85}\text{As}$  (100 and 150 nm) layers. Photoluminescence (PL) measurements qualitatively agree with the HRXRD results.

Various growth interruption (GI) times are introduced after the formation of QDs in order to improve QD uniformity. It is found that a 30-second GI time is the optimum value for the growth of InAs QDs on  $\text{In}_{0.15}\text{Ga}_{0.85}\text{As}/\text{GaAs}$  VS. After InAs QD formation, the QDs are capped with a thin layer of GaAs in order to study the surface evolution with an aim to using it as a template for further QD growth. It is found that nano holes are seen in the middle of the QDs directly grown on GaAs (which has been reported in the literature) but none are seen when the QDs are grown on the cross-hatch VS (which has not been reported). Instead, QDs which are nucleated along the [110] direction become *less* prominent while those nucleated along the [1-10] direction become *more* prominent. This result is attributed to the insufficient and asymmetry of strain energies in the underlying plane on which QDs are grown.

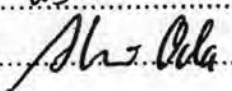
Department.....Electrical Engineering.

Field of study..Electrical Engineering..

Academic year.....2006.....

Student's signature .....  .....

Advisor's signature .....  .....

Co-advisor's signature.....  .....

## Acknowledgements

First I would like to express my greatest gratitude to my advisor, Assoc. Prof. Dr. Songphol Kanjanachuchai for his continuous support in the PhD program. He always teaches me how to ask the questions, shows me the different ways how to solve the research problem and guide me a systematic approach in experimental works and data analysis. Without his guidance and encouragement, I could not have finished the dissertation.

I am also greatly indebted to my co-advisor, Prof. Dr. Shunri Oda, Quantum Nanoelectronics Research Center, Tokyo Institute of Technology (TIT), Japan, who accompanied this work and for a large number of excellent discussions during his short staying in Bangkok.

My special thanks go to Prof. Dr. Somsak Panyakeow, who accepted me as a PhD student and favors me to operate MBE machine in Semiconductor Device Research Laboratory, Department of Electrical Engineering, Faculty of Engineering, Chulalongkorn University. Besides, his helpful comments, discussions, suggestions, and kindness encourage me a full strength to continue doing a research until I finish.

Specifically, I am very grateful to Assoc. Prof. Dr. Montri Sawadsaringkarn for his generous explanations whenever I encounter the problem in Engineering Mathematics and course work. It is a pleasure to acknowledge to Prof. Chua Soo-Jin for his participation as a committee member in this dissertation and Dr. Sakuntam Sanorpim for his fruitful and valuable discussions in XRD results and patient explanations in general idea for MBE growth.

I would like to acknowledge the Japan International Cooperation Agency Office for the South East Asia Engineering Education Development Network of Asean University Network (AUN/SEED-Net), Asian Office for Aerospace Research and Development (AOARD), Thailand Research Fund (TRF), Chulalongkorn University and Nanotech Center (NANOTEC) of Thailand for the financial supports. Finally, I would like to express my adequately gratitude to my parents and all of my associates, Dr. Suwit Kiravittaya, Ms. Suwaree Suraprapapich, Ms. Naparat Siripitakchai, Mr. Supachok Thainoi, Mr. Pornchai Changmong, Mr. Nuttawut Budsayaplakorn and Mr. Teeravat Limwongse who have contributed to this work.

# CONTENTS

page

Abstract (Thai).....	iv
Abstract (English).....	v
Acknowledgements.....	vi
Contents.....	vii
List of Figures.....	x
List of Symbols.....	xix
CHAPTER I Introduction.....	1
CHAPTER II Growth and Characterisation Techniques .....	4
2.1 Molecular Beam Epitaxy (MBE) .....	4
2.1.1 MBE System Overview .....	4
2.1.2 In-Situ Characterisation Tools.....	10
2.1.2.1. Mass Spectroscopy .....	11
2.1.2.2 Reflection High-Energy Electron Diffraction (RHEED) .....	12
2.1.2.2.1 Temperature Calibration .....	13
2.1.2.2.2 Growth Rate Calibration .....	15
2.2 Atomic Force Microscopy (AFM) .....	17
2.3 Photoluminescence (PL) .....	19
2.4 Transmission Electron Microscopy (TEM) .....	20
2.5 X-ray Diffraction (XRD) Technique.....	21
Conclusion.....	23
CHAPTER III Self-Assembled Nanostructures.....	24
3.1 Nature of Low-Dimensional Nanostructures.....	24
3.2 Self-Assembly of Nanostructures .....	27
3.2.1 Self-Assembled Growth .....	28

3.2.1.1 Stranski-Krastanow Mode.....	29
3.2.1.2 Material Consideration.....	31
3.2.2 Theory of Self-Assembled QD Formation.....	32
3.2.2.1 Thermodynamic Analysis.....	33
3.2.2.2 Kinetic Analysis. ....	37
3.3 Defects and Dislocations in Strained Semiconductor	
Heterostructures.....	38
3.3.1 Strain .....	39
3.3.2 Defects .....	43
3.3.2.1 Point Defects .....	43
3.3.2.2 Line Defects or Dislocations .....	43
3.3.2.3 Planar and Volume Defects .....	46
3.3.3 Dislocations .....	46
3.3.3.1 Critical thickness for $\text{In}_x\text{Ga}_{1-x}\text{As}$ growth on GaAs..	47
3.3.3.2 Types of Misfit Dislocations .....	48
3.3.3.3 Surface Steps via Threading Dislocation .....	49
3.3.3.4 Lomer Type Misfit Dislocation .....	51
3.4 Ordered Quantum Dot Growth Techniques .....	52
3.4.1 Growth on Templates .....	52
3.4.1.1 High Index Substrate Template .....	53
3.4.1.2 Undulations Template .....	54
3.4.1.3 Corrugated or Mask Surfaces Template.....	58
3.4.1.4 Superlattice Template .....	60
3.4.2 Growth Techniques.....	61
3.4.2.1 Multi Steps Technique .....	62
3.4.2.2 In-Interruption Growth Technique .....	63
3.4.2.3 Thin-Cap and Regrowth Technique .....	64



3.4.2.4 Atomic Force Tip-Induced Nano-Oxidation, Atomic-Hydrogen Etching/Cleaning and Regrowth Technique.....	65
Conclusion .....	66
 CHAPTER IV Growth and Characterisation of Ordered InAs Quantum Dots on Cross-Hatch Virtual Substrate.....	68
4.1 Structural Characterisation of InGaAs/GaAs Cross-Hatch Virtual Substrates.....	69
4.2 Growth of InAs Quantum Dots on $\text{In}_x\text{Ga}_{1-x}\text{As}$ Cross-Hatch Virtual Substrates.....	75
4.2.1 Effects of Growth Interruption Time.....	76
4.2.2 Effects of Relaxed InGaAs Virtual Substrates .....	80
4.2.3 Effects of In Composition in $\text{In}_x\text{Ga}_{1-x}\text{As}$ Virtual Substrates.....	90
4.2.4 Effects of GaAs Capping Layers.....	93
Conclusion .....	98
 CHAPTER V Conclusions.....	99
 References.....	101
Appendix.....	114
Vitae.....	115

## LIST OF FIGURES

	Page
Figure 2.1	(a) Schematic diagram of the growth chamber and (b) a photograph of RIBER 32P MBE system.....5
Figure 2.2	Temperature profile of the pre-heat process.....6
Figure 2.3	Temperature profile of Ga and In cells. The cells are closed in the dotted line range and opened in solid line range during respective temperature ranges.....7
Figure 2.4	(a) Temperature profile As cell and substrate. The cells are closed in the dotted line range and opened in solid line range during respective temperature ranges.....8
Figure 2.5	(a) Temperature profile for the oxide desorption process and RHEED pattern when the temperature increases and (b) photo taken from the viewport showing RHEED spotty pattern at de-ox temperature (580°C).....9
Figure 2.6	Cross-section of MBE samples grown in order to study the surface morphology of (a) strain relaxed InGaAs layer and (b) QDs formed on strain relaxed layer.....10
Figure 2.7	A schematic diagram of mass spectrometer ( <a href="http://www.stev.gb.com/science/spectroscopy.html">http://www.stev.gb.com/science/spectroscopy.html</a> ) .....11
Figure 2.8	Schematic representation of RHEED geometry showing the incident electron beam at an angle $\theta$ to the surface plane (Herman and Sitter, 1989)..... 13
Figure 2.9	Temperature profile and associated RHEED images during temperature calibration.....14
Figure 2.10	Photos of the RHEED patterns taken from the viewport showing (2×4)-(4×4) reconstruction pattern of GaAs surface.....14
Figure 2.11	Different stages of layer-by-layer growth by nucleation of 2D islands and the corresponding intensity of the zero-order diffracted RHEED beam (Franchi et al., 2003).....15
Figure 2.12	Dependence of growth rates of (a) GaAs on the Ga temperature

	and (b) InAs on the In temperature. BEP of As <sub>4</sub> source is kept at $3.5 \times 10^{-6}$ Torr and the BP during growth is $\sim 10^{-7}$ Torr.....	17
Figure 2.13	Schematic drawing of AFM experimental set up (Allen Timothy Chang, UC Berkeley, 2002).....	18
Figure 2.14	Photo of the AFM machine (SPA-400 SPM unit).....	18
Figure 2.15	Schematic diagram of PL experimental set up.....	19
Figure 2.16	Ray diagram of a conventional transmission electron microscopy (Poole and Owens, 2003). The selected area electron diffraction (SAED), aperture (Ap), the sample, the objective (Obj) and projector (Proj) are indicated.....	20
Figure 2.17	Photo of the JEOL JEM-2010 electron microscope.....	21
Figure 2.18	Reflection of X-ray beam incident at the angle $\theta$ off two parallel planes separated by the distance (d).....	22
Figure 2.19	Photo of the (D8 BRUKER) X-ray Diffractometer System.....	23
Figure 3.1	Schematic comparison of typical dimensions of bulk material, waveguide for visible light, a QD and an atom (Bimberg et al., 1999).....	25
Figure 3.2	Nature of electronic states in bulk, quantum well and quantum dot. Top row: schematic morphology, center row: quantized electronic states, bottom row: density of electronic states (Bimberg et al., 1999).....	27
Figure 3.3	Schematic representation of the three crystal growth modes of a film for a different coverage ( $\theta$ ) (a) layer-by-layer or Frank-van der Merwe (b) layer-plus-island or Stranski-Krastanow mode island and (c) Volmer-Weber (Herman and Sitter, 1989).....	29
Figure 3.4	Schematic representation of total energy change for a strained system in 2D- and 3D- growth modes. $t_{cw}$ and $t_{cd}$ are critical thicknesses for formation of islands and dislocations, respectively (Seifert et al., 1996).....	30
Figure 3.5	Schematic illustration of total energy as a function of time for the	

	2D-3D morphology transition. A: 2D layer-by-layer growth, B: 2D-3D transition, C: ripening period, $t_{cw}$ : critical wetting layer thickness, $E_A$ : barrier for formation of 3D islands, X: point where a pure strain-induced transition becomes possible, and between X and Y: a slow ripening process continues (Seifert et al., 1996).....	31
Figure 3.6	Energy gap versus lattice constant for most commonly used semiconductors.....	32
Figure 3.7	Energy of an array of 3D coherently strained islands per one atom versus size of the atom. The control parameter $\alpha$ is the ratio of the surface energy and edge energy (Bimberg et al., 1999).....	33
Figure 3.8	Equilibrium phase diagram of a lattice-mismatched heteroepitaxial system as a function of epilayer thickness $H$ and the lattice mismatch. The small panels on the top and bottom illustrate the morphology of the surface in the six growth modes. The small empty triangles represent the presence of stable islands, while the large shaded area ones refer to ripened islands (Daruka and Barabási, 1997).....	36
Figure 3.9	Schematic representation of the local strain energy density in and around the 3D island. (Seifert et al., 1996) .....	38
Figure 3.10	Schematic representations of (a) unstrained layer, (b) compressive strained layer and (c) tensile strained layer. The opened squares represent atoms of the substrate materials and closed squares are atoms of the epitaxial materials. In (b) and (c) the lattice constants of the epitaxial layers are different from the substrate materials. The arrows in (b) and (c) represent forces (stresses) exerted on the epitaxial layer.....	40
Figure 3.11	(a) diffraction peaks from the epitaxial layer (at $\theta_c$ ), and	

	(b) the substrate (at $\theta_s$ ).....	40
Figure 3.12	Theoretical graph for critical thickness of InGaAs as a function of strain (Fritz et al., 1985).....	42
Figure 3.13	Schematic diagram showing point defects in a crystal (Singh, 2003).43	
Figure 3.14	Schematic representation of (a) edge dislocation and (b) screw dislocation ( <a href="http://en.wikipedia.org/wiki/Dislocation#Edge_dislocations">http://en.wikipedia.org/wiki/Dislocation#Edge_dislocations</a> ).....	44
Figure 3.15	Dislocation geometry in heteroepitaxial mismatched thin films. (a) One of the inclined {111} planes for a (001) oriented fcc film/substrate system with a gliding TD segment and a trailing MD. (b) Dislocation Burgers (Andrew et al., 2002) .....	45
Figure 3.16	Burgers circuit (a) around a dislocation and (b) in a perfect crystal (Hull, 1965).....	46
Figure 3.17	Critical thickness for defect introduction for $\text{In}_x\text{Ga}_{1-x}\text{As}$ on GaAs.....	47
Figure 3.18	Geometric of appearance of surface step via gliding of threading dislocation with Burgers vector $b$ (Hongland et al., 2004).....	49
Figure 3.19	TEM images showing dislocation observed in GaAs/ $\text{In}_{0.15}\text{Ga}_{0.85}\text{As}$ /GaAs for various thicknesses ( $h$ ) of InGaAs layers (a) misfit dislocation segment ( $h=6$ nm) (b) elongated misfit dislocation segment (15 nm) and (c) misfit dislocation network with threading dislocation ( $h=25$ nm) (Liu et al., 1999).....	50
Figure 3.20	(a) AFM and (b) TEM images of cross-hatch pattern for $\text{In}_{0.25}\text{Ga}_{0.75}\text{As}$ /GaAs (001) (Yastrubchak et al., 2003).....	50
Figure 3.21	TEM image showing V-shape configuration resulted from inclined slip loops originating in misfit dislocation network	

	(Rajan et al., 1987).....	51
Figure 3.22	Schematic drawing of the spatial dislocation configuration for the case of L-MD which is commonly found in pure edge MD (Vdovin, 1997).....	52
Figure 3.23	AFM images of (2 $\mu\text{m} \times 2 \mu\text{m}$ ) of the QD layers grown on (a) GaAs (100), (b) GaAs (911)B, (c) GaAs (711)B, (d) GaAs (511)B, (e) GaAs(411)B and (f) GaAs (311)B (Wang et al., 2005).....	53
Figure 3.24	(a) AFM and (b) cross-sectional TEM images of a 15 ML of InP QDs grown on 150-nm thick $\text{In}_{0.61}\text{Ga}_{0.39}\text{P}$ layer (Häusler et al., 1996) .....	54
Figure 3.25	(a) schematic display of a relaxed template of SiGe based on a Si (100) substrate and (b) AFM image (10 $\mu\text{m} \times 10 \mu\text{m}$ ) of Ge islands on the Si layer above a misfit dislocation network (Xie et al., 1997).....	55
Figure 3.26	Images of InAs QDs on (a) 162 nm and (b) 325 nm of $\text{In}_{0.15}\text{Ga}_{0.85}\text{As}$ layers (Hiwatachi et al., 1997).....	56
Figure 3.27	(a) A cross-sectional TEM image showing vertically 3 stacked InAs QDs on a strained layer with $n$ is 25 and misfit dislocations and (b) $0.5 \times 0.5 \mu\text{m}^2$ AFM image of 1.6 ML of InAs QDs arrays grown on strain-engineered superlattice template with $n$ is 30 (Kim et al., 2004).....	56
Figure 3.28	AFM images of (a) 0.8 ML, (b) 2 ML of InAs QDs on 50-nm $\text{In}_{0.15}\text{Ga}_{0.85}\text{As}$ layer and (c) 2 ML of InAs QDs on 180-nm $\text{In}_{0.15}\text{Ga}_{0.85}\text{As}$ layer (Zhang et al., 2006).....	57
Figure 3.29	Graph of surface stress as a function of lateral distance from misfit dislocation ( $\sigma_{xx}$ ) showing the reason of the ordering of QDs is weak when the InGaAs layer is relatively thick (Zhang et al., 2006).....	57
Figure 3.30	AFM images of InAs QDs aligned along the (a) [011] and (b) [01-1]	

	oriented ridges (Mui et al., 1995).....	58
Figure 3.31	AFM image of V-grooves InAs islands aligned along [01-1] oriented ridges (Mui et al., 1995).....	59
Figure 3.32	(a) Three dimensional display of an AFM image of a 450 nm wide Si ridge along <100>. Ge islands line up along the edges of the mesa. (b) The corresponding cross-sectional of schematic (Kamins et al., 1997).....	59
Figure 3.33	AFM images of (a) 6 ML in different scales and (b) and (c) are shown in different scales of In <sub>0.5</sub> Ga <sub>0.5</sub> As QD multilayers (Wang et al., 2004) .....	60
Figure 3.34	AFM images of the surfaces during formation of the 16 <sup>th</sup> period of the (In,Ga)As 2.3nm/GaAs 13.0 nm QWR template (a) 2.3 nm In <sub>0.41</sub> Ga <sub>0.59</sub> As grown at 540°C (b) 0.7 nm GaAs cap deposited at 540°C without growth interruption (c) annealing at 580°C for 2 min and (d) 12.3 nm GaAs grown at 580°C (Mano et al., 2004).....	61
Figure 3.35	AFM image (300 nm×300 nm) of InGaAs quantum dots aligned multiaatomic steps on GaAs (001) surface misoriented by 2° toward [101] direction (Kitamura et al., 1995).....	62
Figure 3.36	AFM image (a) of multiaatomic steps on GaAs layer grown on a vicinal (111)B GaAs and (b) InGaAs islands by growing 3-nm-thick In <sub>0.3</sub> Ga <sub>0.7</sub> As layer onto GaAs multiaatomic sites (Akiyama et al., 2006).....	63
Figure 3.37	(a) Schematic drawing of In-interruption growth technique and (b) AFM image (3000 nm×3000 nm) of InAs QDs with a In-interruption time 9 sec (Hong et al., 2006).....	64
Figure 3.38	AFM images of (a) nanohole (b) 1 cycle (c) 7 cycles of thin-cap and regrowth of QDs on nanoholes (Suwaree et al., 2006) .....	65
Figure 3.39	The schematic illustration of the experimental processes for (a) the formation of the nano-oxide dots on GaAs (001) surface by	

	AFM tip-induced oxidation, (b) the subsequent removal of a nano-oxide dot and native oxide layer by atomic hydrogen droplet epitaxy.....	66
Figure 3.40	AFM images of (a) nano-oxide dots (b) nanoholes and (c) InAs QD arrays grown by droplet epitaxy (Kim et al., 2006).....	66
Figure 4.1	AFM image of the surface of In <sub>0.15</sub> Ga <sub>0.85</sub> As layer on GaAs (001) substrate.....	70
Figure 4.2	FFT analysis of 25×25 μm <sup>2</sup> In <sub>0.15</sub> Ga <sub>0.85</sub> As layer on GaAs substrate along [1-10] direction.....	72
Figure 4.3	(a) Cross-sectional TEM image of In <sub>0.15</sub> Ga <sub>0.85</sub> As/GaAs layer and (b) the growth structure.....	73
Figure 4.4	HRXRD (004) 2θ/ω spectrum of 50 nm InGaAs layer grown on GaAs (001) substrate.....	74
Figure 4.5	Low temperature (77K) photoluminescence spectrum of In <sub>0.15</sub> Ga <sub>0.85</sub> As layers grown on GaAs (001) substrate.....	75
Figure 4.6	AFM images of InAs QDs grown on InGaAs/GaAs with growth interruption times of (a) 0 sec, (b) 30 sec and (c) 60 sec. The height contrast is 8.5 nm.....	76
Figure 4.7	AFM images of the (a) surface of In <sub>0.15</sub> Ga <sub>0.85</sub> As layer on GaAs (001) substrate and (b) InAs QDs grown on In <sub>0.15</sub> Ga <sub>0.85</sub> As/GaAs with growth interruption times of 30 sec. All images are 25×25 μm <sup>2</sup> in size and the arrows point towards the [1-10] direction.....	77
Figure 4.8	Density of QDs on cross hatch with a function of growth interruption time taken from the 3×3 μm <sup>2</sup> by counting the dots along the [1-10] and [110] direction on cross-hatch VS.....	78
Figure 4.9	(a) AFM image of InAs QDs aligned along [1-10] direction and (b) the orientation of the dots. The arrow indicates [1-10] direction...	79
Figure 4.10	Distribution of the width of QDs on VS along the (a) [1-10] and (b) [110] directions.....	80
Figure 4.11	AFM images of InAs QDs grown on In <sub>0.15</sub> Ga <sub>0.85</sub> As/GaAs	



	virtual substrate where the thickness of the $\text{In}_{0.15}\text{Ga}_{0.85}\text{As}$ layer is (a) 50 nm, (b) 100 nm and (c) 150 nm. The arrows point towards the [1-10] direction.....	81
Figure 4.12	Line scans (2.5 $\mu\text{m}$ ) along the [1-10] direction taken on a ridge (upper lines) or between ridges (lower) of the cross hatch where InAs QDs are formed on virtual substrates with InGaAs layer thickness of (a) 50-, (b) 100- and (c) 150 nm.....	83
Figure 4.13	(a) HRXRD (004) $2\theta/\omega$ curves and (b) the deduced lattice constants ( $a_L$ ) of the three samples with $\text{In}_{0.15}\text{Ga}_{0.85}\text{As}$ layer thickness of 50-, 100- and 150 nm.....	84
Figure 4.14	HRXRD (115) $2\theta/\omega$ curves of the three samples with $\text{In}_{0.15}\text{Ga}_{0.85}\text{As}$ layer thickness of 50-, 100- and 150 nm.....	85
Figure 4.15	A profile showing percent relaxation as a function of $\text{In}_{0.15}\text{Ga}_{0.85}\text{As}$ layers with various thicknesses.....	86
Figure 4.16	Low temperature (77 K) PL spectra of InAs quantum dots grown on partially relaxed $\text{In}_{0.15}\text{Ga}_{0.85}\text{As}$ layers with various thicknesses of 50-, 100- and 150 nm.....	87
Figure 4.17	Low temperature (77 K) PL emission peak of InAs QDs grown on partially relaxed $\text{In}_{0.15}\text{Ga}_{0.85}\text{As}/\text{GaAs}$ VS as a function of calculated percent relaxation of InGaAs strained layers.....	88
Figure 4.18	Cross-sectional schematic diagram of the evolution of InAs QDs on (a) 50-, (b) 100- and (c) 150-nm InGaAs virtual substrate.....	89
Figure 4.19	25 $\times$ 25 $\mu\text{m}^2$ AFM images of InAs QDs grown on $\text{In}_x\text{Ga}_{1-x}\text{As}$ layers where x is equal (a) 0.10, (b) 0.13 and (c) 0.15.....	90
Figure 4.20	The density of cross hatch as a function of In composition.....	91
Figure 4.21	The density of QDs as a function of In composition.....	91
Figure 4.22	(a) HRXRD (004) $2\theta/\omega$ curves of InAs QDs grown on 50-nm InGaAs layer with various In composition of 0.10, 0.13 and 0.15 (b) the deduced lattice constants ( $a_L$ ) of the three samples with 50-nm $\text{In}_x\text{Ga}_{1-x}\text{As}$ layer (x=0.10, 0.13, and 0.15).....	92

Figure 4.23	AFM images of (a) as grown InAs QDs on GaAs substrate, (b) nano propeller structure created by capping the as grown QDs with 9 ML of GaAs layer and (c) regrown QDs on the nano propeller template.....	94
Figure 4.24	Line scan of InAs QDs capped partially with 9 ML of GaAs layer.....	94
Figure 4.25	(a) $3 \times 3 \mu\text{m}^2$ AFM images of 0.8 ML of InAs QDs grown on 50-nm $\text{In}_{0.15}\text{Ga}_{0.85}\text{As}/\text{GaAs}$ VS and capped partially with (b) 2 ML GaAs layers. The second rows and the third rows show the cross-sectional view of nanostructure for each corresponding AFM image along [1-10] and [110] directions.....	95
Figure 4.26	$3 \times 3 \mu\text{m}^2$ AFM images of 0.8 ML of InAs QDs grown on 50-nm $\text{In}_{0.15}\text{Ga}_{0.85}\text{As}/\text{GaAs}$ VS and capped partially with (a) 2 ML and (b) 6 ML GaAs layers. The second rows and the third rows show the cross-sectional view of nanostructure for each corresponding AFM image along [1-10] and [110] directions.....	96
Figure 4.27	AFM image of InAs regrown QDs on 50-nm $\text{In}_{0.15}\text{Ga}_{0.85}\text{As}/\text{GaAs}$ cross-hatch VS capped partially with 6 ML of GaAs.....	97

$a_l$	lattice constant of overlayer
$a_s$	lattice constant of substrate
AFM	atomic force microscopy
As	arsenic
$b_e$	edge Burger's vector component
$b_s$	screw Burger's vector component
$b_{  }$	parallel Burger vector
$b_{\perp}$	perpendicular Burger vector
BEP	beam equivalent pressure
BP	background pressure
$C$	elastic constant
CO	carbon monoxide
$\delta$	delta function
$D_{bulk}(E)$	bulk density of state
$D_{QD}(E)$	quantum dot density of state
$D_{QW}(E)$	quantum well density of state
$D_{QWR}(E)$	quantum wire density of state
DFM	dynamic force microscopy
$E_0$	characteristic energy
$E_A$	barrier for formation of islands
$E_c$	conduction band energy
$E_{edge}$	edge energy
$E(el)$	elastic strain energy
$E_{elastic}$	elastic energy
$E_g$	energy gap
$E_{st}$	strain energy
$E_{surf}$	surface energy
FM	Frank-van der Merwe
Ga	gallium
GaAlAsP	gallium aluminum arsenide phosphide

GaAs	gallium arsenide
GaSb	gallium antimonite
Ge	germanium
GI	growth interruption
$h$	Planck's constant
$h_c$	critical thickness
HRXRD	high resolution X-ray diffraction
In	indium
InGaAs	indium gallium arsenide
InP	indium phosphide
$\mathbf{k}=(k_x, k_y, k_z)$	carrier wave vector
$k_B$	Boltzmann's constant
$k_{  }$	amplitude of in-plane (y-z) wave vector
$k_{\perp}$	amplitude of wave vector in x-direction
$l$	quantum number in x-direction
$\lambda$	elastic modulus
$L_0$	characteristic length
$LN_2$	liquid nitrogen
LPE	liquid phase epitaxy
$m$	quantum number in y-direction
ML	monolayer
$m/z$	mass-to-charge ratio
$n$	quantum number in z-direction
$N_D$	volume density of quantum dot
$N_{wi}$	area density of quantum wire
$m^*$	effective mass
$m_{eff}$	effective mass of carrier
MBE	molecular beam epitaxy
MD	misfit dislocation
MO	molybdenum block
MOCVD	metal organic chemical vapor deposition
$p$	momentum

PL	photoluminescence
RHEED	reflection high-energy electron diffraction
$T_{\text{std}}$	standby temperature
$T_{\text{sub}}$	substrate temperature
QD	quantum dot
QW	quantum well
QWR	quantum wire
$\rho$	island density
$r_f$	film surface energy
$r_i$	interface energy between the film and substrate
$r_s$	substrate surface energy
$R_{\text{GaAs}}$	growth rate of gallium arsenide
$R_{\text{InAs}}$	growth rate of indium arsenide
$R_{\text{InGaAs}}$	growth rate of indium gallium arsenide
$\sigma$	Poisson ratio
$\epsilon$	lattice mismatch or strain
SAQD	self assembled quantum dot
SK	Stranski-Krastanow
SL	superlattice
Si	silicon
SiGe	silicon germanium
$t$	film thickness
$t_{cd}$	critical thickness for formation of dislocations
$t_{cw}$	critical thickness for formation of islands
$T$	temperature
TD	threading dislocation
$\theta_e$	diffraction angle from epilayer
$\theta_s$	diffraction angle from substrate
$\Theta$	Heaviside's unit step function
TEM	transmission electron microscopy
VPE	vapor phase epitaxy
VS	virtual substrate

VW	Volmer-Weber
WL	wetting layer
$x_0$	island size
XRD	X-ray diffraction